On the identification of diffuso-mechanical properties of polymer matrix materials based on the use of plates with asymmetric moisture concentration field

Djato A., Beringhier M., Gigliotti M.

On the identification of diffuso-mechanical properties of polymer matrix materials based on the use of plates with asymmetric moisture concentration field

Djato A.[a,*], Beringhier M.[a], Gigliotti M.[a]

[a] *Institut P', CNRS - ISAE ENSMA - Université de Poitiers, Département Physique et Mécanique des Matériaux, ENSMA, Téléport 2, 1 avenue Clément Ader, BP 40109, 86961 Futuroscope Chasseneuil Cedex, France*

Abstract

The aim of the paper is to investigate the possibility to identify the moisture affected mechanical properties and the coefficient of moisture expansion of polymer matrix materials using plates subject to asymmetric concentration field. The study is performed on samples with thin plate configuration using a weakly coupled diffuso-mechanical model: 1D Fick's diffusion model and 2D plane stress hygroelastic model. Because of the intensity of the deflections caused by the asymmetry of the concentration field, the use of a model taking into account geometrical non-linearities is discussed. The identification is performed according to a constant and linear dependence of Young's modulus on moisture content. It is shown that diffuso-mechanical properties and the coefficient of moisture expansion can be simultaneously identified by using geometrically linear and non-linear approaches.

Keywords: Polymer matrix material, Identification, diffuso-mechanical model, asymmetric concentration field, Rayleigh-Ritz method

*Corresponding author
Email address: anani.djato@ensma.fr (Djato A.)

List of symbols

Notation	Defintion
$(x,\, y,\, z)$	Coordinates along the $\overrightarrow{x}$, $\overrightarrow{y}$ and $\overrightarrow{z}$ directions
$(L_x,\, L_y,\, L_z)$	Length along the x, y and z directions (mm)
$(X,\, Y,\, Z)$	$[-\frac{L_x}{2}; \frac{L_x}{2}]$, $[-\frac{L_y}{2}; \frac{L_y}{2}]$ and $[-\frac{L_z}{2}; \frac{L_z}{2}]$ interval
$\rho,\, V$	Material density (g.mm^{-3}), volume (mm^3)
T	Temperature ($^\circ C$)
RH	Relative humidity (%)
β	Coefficient of moisture expansion
D_{zz}	Diffusion coefficient along the thickness
$(C,\, C_i)$	Current and initial moisture concentrations (g.mm^{-3})
$(C_1^\infty,\, C_2^\infty)$	Boundary concentrations at $z = -\frac{L_z}{2}$ and $z = \frac{L_z}{2}$ (g.mm^{-3})
$(m,\, m_0)$	Current and initial moisture contents
$\overline{m}$	Average of moisture content along the thickness
$(m_1^\infty,\, m_2^\infty)$	Boundary moisture content at $z = -\frac{L_z}{2}$ and $z = \frac{L_z}{2}$
$\mathbf{E}^0$ $(\varepsilon^0_{xx},\, \varepsilon^0_{xy},\, \varepsilon^0_{zz})$	Membrane in-plane strain tensor (components of $\mathbf{E}^0$)
$\mathbf{E}^H$ $(\varepsilon^H_{xx},\, \varepsilon^H_{xy},\, \varepsilon^H_{zz})$	Hygroscopic strain tensor (components of $\mathbf{E}^H$)
$\mathbf{E}$ $(\varepsilon_{xx},\, \varepsilon_{xy},\, \varepsilon_{zz})$	Strain tensor (components of $\mathbf{E}$)
$\mathbf{K}$	Curvature tensor
$\mathbf{Q}$	Elasticity tensor
$(E,\, E(m))$	Young's modulus, possibly depending on m
$(\alpha,\, \eta)$	Parameters such as $E(m) = \alpha m + \eta$
$(\nu,\, \nu(m))$	Poisson's ratio, possibly depending on m
$Q(m)$	Notation for $\frac{E(m)}{1-\nu(m)^2}$
$(e^d,\, E^d,\, E^{ext},\, E^{tot})$	Strain energy density, strain energy, work of external efforts, total potential energy
$\Phi(x, y, z)$	Interpolation functions
$U(x, y, z,)$	General representation of displacement
$(a,\, b,\, c,\, d)$	Displacement parameters for the Rayleigh-Ritz method
$(u(x, y),\, v(x, y))$	In-plane displacement fields
$w(x, y)$	Out-of-plane displacement field

1. Introduction

Organic Matrix Composite (OMC) materials are increasingly used in the industrial sector, in particular in the aeronautical industry for realization of warm structural ($50°C < T < 300°C$) parts. In these parts, including in particular turboengines and nacelles, exposition to aggressive environments may lead to the diffusion of species (H_2O, O_2,...) in the polymeric matrix. Under these circumstances, degradation phenomena related to the action of thermomechanical and/or chemo-diffuso-mechanical coupling phenomena can occur affecting their durability (Weitsman, 2012). Humid aging of OMC ($50°C < T < 100°C$) is of particular concern for the aeronautical industry; the diffusion of water in the polymer matrix of the composite (fibrous carbon reinforcements usually employed in aeronautical industry do not absorb water) may promote hygroscopic swelling and changes in mechanical properties (stiffness, strength) (Weitsman, 2012; Shen and Springer, 1976, 1977a,b; Simar, 2014). Numerical and experimental models are developed to identify mechanical properties in humid environments. The identification of the moisture affected mechanical behavior of polymer matrix materials is usually carried out on moisture-saturated samples (Shen and Springer, 1977a; Simar et al., 2014; Simar, 2014). In the work by Simar et al. (Simar et al., 2014) and Simar (Simar, 2014), tensile tests have been carried out on moisture-saturated thin plate RTM6 samples (4mm thickness) at distinct relative humidity (RH%) and at fixed temperature, T = 70°C, leading to the identification of the elastic properties such as Young's modulus, E, and Poisson's ratio, ν, as a function of the saturation moisture content, m_∞. These tests require a large number of samples and long conditioning and identification times since moisture-saturated samples are considered (in (Simar, 2014), about 1500h for each sample with 4mm thickness). In our previous work, (Djato et al., 2018), a numerical study allowing to identify moisture affected mechanical properties of polymer matrix materials has been established. The study was based on tensile and bending tests on samples with moisture gradients and led to a significant reduction of identification time compared to moisture-saturated samples.

However, the use of tensile and bending tests failed to identify the coefficient of moisture expansion β due to the dependence of the measured residual strains on β. In the literature ((Simar et al., 2014), (Obeid et al., 2018)), direct identifications of β are carried out using the change in volume measurement of the plate. Though, a protocol allowing simultaneous identification of the diffuso-mechanical properties and the coefficient of moisture expansion on saturated samples as on samples with moisture gradients has never been implemented.

The aim of the paper is to investigate the possibility to identify the moisture affected mechanical properties and the coefficient of moisture expansion of polymer matrix materials using plates subject to asymmetric concentration field. The study is performed on samples with thin plate configuration using a weakly coupled diffuso-mechanical model: 1D Fick's diffusion model describing the kinetics of diffusion and 2D plane stress hygroelastic model whose numerical solutions are carried out by the finite difference method and the Rayleigh-Ritz method, respectively. Because of the intensity of the deflections promoted by the asymmetry of the concentration field, the use of a model taking into account geometrical non-linearities is discussed. Imposing different concentrations on the two opposite surfaces of the plate induces an asymmetric distribution of water concentration along the thickness and generates deflections of the plate. These deflections (strains and curvatures) may be used to perform identification in a transient state. The results of the identification are illustrated for constant and linear dependences of Young's modulus on moisture content. The conclusions of the present study will be used for designing a proper test (sample dimensions and humidity conditions) starting from the knowledge of the moisture dependent material properties identified by using traction tests. Gigliotti et al. (see (Gigliotti et al., 2006), (Gigliotti et al., 2007)) have carried out tests on 0/90 unsymmetric composite samples exposed to transient and cyclical humid homogeneous conditions. In that case, the deflection of the samples was generated by the unsymmetry of the structural configuration instead of the unsymmetry of the moisture distribution. However a similar effect (at least qualitatively) can be expected. This will be checked further. It should be also emphasized

that the possibility to carry out sorption tests with different concentration values on the two opposite surfaces, was explored experimentally by Ounaies et al. (Ounaies et al., 2018). The present work is organized as follows. Section 2 is devoted to the presentation of the coupled diffuso-mechanical model with presentation of Rayleigh-Ritz method adapted for thin plates. In section 3, the direct problem is illustrated in geometrically linear and non-linear approaches. In section 4, the inverse problems are presented followed by numerical results in section 5 for geometrically linear and non-linear approaches with consideration of some particular dependences of Young's modulus on the moisture content. Section 6 presents discussions on the identified parameters while section 7 presents conclusions and perspectives of the present research.

2. Thin plate diffuso-mechanical model

Fully coupled diffuso-elasticity is discussed for instance in (Youssef et al., 2009), but, for setting up a starting experience, by using a simplifying hypothesis, an uncoupled approach was used in the present paper. The simplifying hypotheses of the uncoupled approach are used to setup an experiment using thin plates in the geometrically nonlinear regime. This study was carried out by considering polymer matrix thin plates (Fig.1) configuration with the assumption that species diffusion is essentially unidirectional along the thickness direction governed by 1D Fick's diffusion model. This diffusion model is associated with a 2D plane stress hygroelastic thin plate model. The moisture concentration field is determined firstly by solving 1D Fick's equation, then moisture content is input within the 2D hygroelastic model for strains and stresses calculations.

2.1. 1D *Fick's diffusion model*

Since the material is homogeneous and isotropic in thin plate configuration, the water is supposed to diffuse only in the thickness direction denoted by z. The water diffusion kinetics is described by the Fick's law (Fick, 1855) and is

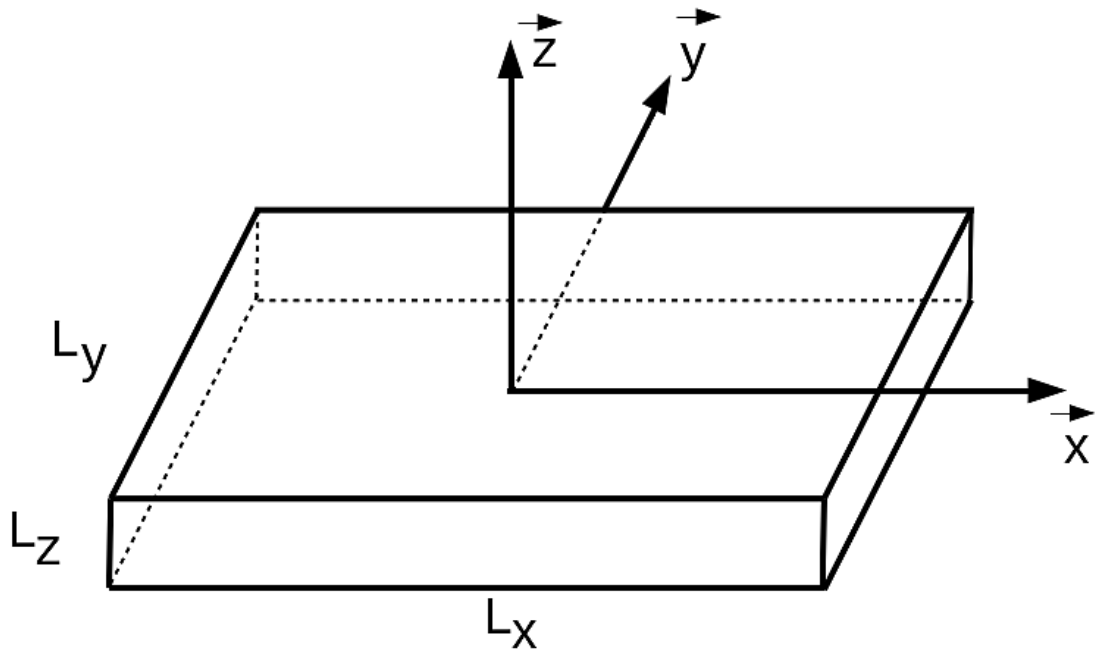

Figure 1: Plate geometry

written as follows

$$\begin{cases} \dfrac{\partial C}{\partial t}(t,z) = D_{zz}\dfrac{\partial^2 C}{\partial z^2}(t,z) \\ C(0,z) = C_i;\ \forall z \in Z = [-\dfrac{L_z}{2};\dfrac{L_z}{2}] \\ C(t,-\dfrac{L_z}{2}) = C^1_\infty;\ \forall t > 0 \\ C(t,\dfrac{L_z}{2}) = C^2_\infty;\ \forall t > 0 \end{cases} \tag{1}$$

where C is the moisture concentration field, L_z is the plate thickness, C^1_∞ is the value of the moisture concentration field imposed on the lower edge ($z = -\frac{L_z}{2}$), C^2_∞ ($C^2_\infty \neq C^1_\infty$) is the value of the moisture concentration field imposed on the upper edge ($z = \frac{L_z}{2}$), C_i is the initial moisture concentration (at $t = 0$) and D_{zz} is the diffusion coefficient along the thickness. The analytical solution exists only for uniform boundary conditions all over the edges. In this study, a numerical solution is computed by the finite difference method. By assuming that there is no moisture in the initial state, $C_i = C(0,z) = 0;\ \forall z \in Z = [-\frac{L_z}{2};\frac{L_z}{2}]$, the moisture content denoted by $m(t,z)$ is then given by

$$m(t,z) = \frac{C(t,z)}{\rho} \tag{2}$$

where ρ represents material density. The diffusion properties are not the subject of the identification problem in this paper and are assumed as known (see the work of Beringhier et al., (Beringhier et al., 2018)). In this paper, the moisture content, m, will be assumed as function of time and of the position along the thickness direction ($m = m(t,z)$) and its average along the thickness, $\overline{m}$, will be a function of time only ($\overline{m} = \overline{m}(t) = \frac{1}{L_z}\int_Z m(t,z)dz$). These quantities are assumed as known.

2.2. 2D *plane stress hygroelastic model*

In the geometrically non-linear theory of plates, also called Von Kármán model for plates, (Zara, 2017; Hyer, 1981), the strain tensor is given by

$$\mathbf{E} = \mathbf{E}^0 - z\mathbf{K} \tag{3}$$

where $\mathbf{E}^0$ is the membrane in-plane strain tensor given by

$$\mathbf{E}^0 = \begin{cases} \varepsilon^0_{xx} = \dfrac{\partial u}{\partial x} + \dfrac{1}{2}(\dfrac{\partial w}{\partial x})^2 \\ \varepsilon^0_{yy} = \dfrac{\partial v}{\partial y} + \dfrac{1}{2}(\dfrac{\partial w}{\partial y})^2 \\ 2\varepsilon^0_{xy} = \dfrac{\partial u}{\partial y} + \dfrac{\partial v}{\partial x} + (\dfrac{\partial w}{\partial x})(\dfrac{\partial w}{\partial y}) \end{cases} \tag{4}$$

with ε^0_{xx} and ε^0_{yy} being the membrane longitudinal and transverse in-plane strains and ε^0_{xy} the shear strain. The longitudinal in-plane displacement field u and the transverse in-plane displacement field v of the middle plane ($z = 0$) depend only on x and y (Zara, 2017) as well as the out-of-plane displacement field w whereas $(\frac{\partial w}{\partial x})^2$, $(\frac{\partial w}{\partial y})^2$ and $(\frac{\partial w}{\partial x})(\frac{\partial w}{\partial y})$ represent the non-linear parts. The tensor $\mathbf{K}$ represents the curvatures of the plate on the middle plane. Due to the assumption of moderate rotations, the non-linear expressions are neglected with respect to unity and $\mathbf{K}$ is reduced to Eq.(5)

$$\mathbf{K} = \begin{cases} k_{xx} = \dfrac{\frac{\partial^2 w}{\partial x^2}}{[1 + (\frac{\partial w}{\partial x})^2]^{\frac{3}{2}}} \simeq \dfrac{\partial^2 w}{\partial x^2} \\ k_{yy} = \dfrac{\frac{\partial^2 w}{\partial y^2}}{[1 + (\frac{\partial w}{\partial y})^2]^{\frac{3}{2}}} \simeq \dfrac{\partial^2 w}{\partial y^2} \\ 2k_{xy} = \dfrac{\frac{\partial^2 w}{\partial x \partial y}}{[1 + (\frac{\partial w}{\partial x})(\frac{\partial w}{\partial y})]^{\frac{3}{2}}} \simeq \dfrac{\partial^2 w}{\partial x \partial y} \end{cases} \tag{5}$$

where k_{xx} and k_{yy} are the longitudinal and transverse curvatures of the plate and k_{xy} is the shear curvature. The 2D plane stress hygroelastic model describing the plate behavior is coupled to the diffusion model through the dependences of the mechanical properties and the hygroscopic strains on the moisture content, m, as follows

$$\boldsymbol{\sigma} = \mathbf{Q}(m)(\mathbf{E} - \mathbf{E}^H) \tag{6}$$

$\mathbf{Q}(m)$ is the elasticity tensor under the plane stress assumption, that is,

$$\mathbf{Q}(m) = \begin{bmatrix} Q(m) & \nu(m)Q(m) & 0 \\ \nu(m)Q(m) & Q(m) & 0 \\ 0 & 0 & \frac{1}{2}(1-\nu(m))Q(m) \end{bmatrix} \tag{7}$$

with $Q(m) = \frac{E(m)}{1-\nu(m)^2}$. The material parameters ν and E depend on the moisture content. The hygroscopic strain tensor $\mathbf{E}^H$ is given by

$$\mathbf{E}^H = \begin{cases} \varepsilon^H_{xx} = \beta\Delta m \\ \varepsilon^H_{yy} = \beta\Delta m \\ \varepsilon^H_{xy} = 0 \end{cases} \tag{8}$$

where β is the coefficient of moisture expansion and $\Delta m = m - m_0$ is the change of moisture content from an initial reference value, m_0, to the current state, m. The coefficient of moisture expansion can depend on m, but it is usually assumed constant for polymers and polymer matrix materials (Simar, 2014).

2.3. Energy minimization problem and Rayleigh-Ritz method

The hygroelastic 2D plane stress problem can be solved by employing the Rayleigh-Ritz method (Djato et al., 2018; Mansfield, 1989). The first step is to define the total potential energy of the plate as

$$E^{tot} = E^d + E^{ext} \tag{9}$$

where E^d is the strain energy and E^{ext} is the external work due to external loadings. The strain energy is given by

$$E^d = \int_V e^d dV \tag{10}$$

with e^d being the strain energy density given by

$$e^d = \frac{1}{2}\mathbf{E} \cdot \mathbf{Q}(m)\mathbf{E} - \mathbf{E}^H \cdot \mathbf{Q}(m)\mathbf{E} \tag{11}$$

where V is the plate volume.

By introducing the expressions of $\mathbf{Q}(m)$ (Eq.(7)) and $\mathbf{E}$ (Eq.(3)) into Eq.(11), we have

$$\begin{aligned} e^d = & Q(m)[(\varepsilon^0_{xx} - zk_{xx})^2 + (\varepsilon^0_{yy} - zk_{yy})^2 + 2(1-\nu(m))(\varepsilon^0_{xy} - zk_{xy})^2] \\ & + 2\nu(m)Q(m)(\varepsilon^0_{xx} - zk_{xx})(\varepsilon^0_{yy} - zk_{yy}) \\ & - \beta\Delta m Q(m)(1-\nu(m))[(\varepsilon^0_{xx} - zk_{xx}) + (\varepsilon^0_{yy} - zk_{yy}) + (\varepsilon^0_{xy} - zk_{xy})] \end{aligned} \tag{12}$$

The minimization problem describing the stable equilibrium positions of the plate is given by

$$\begin{cases} \delta E^{tot} = 0 \\ \delta^2 E^{tot} > 0 \end{cases} \tag{13}$$

where only stable solutions are sought (those who satisfy the second equation of Eq.(13)). By using Eq.(4) and Eq.(5), the first equation of Eq.(13) leads to a non-linear partial differential equation (PDE) under a variational form where the unknowns are the displacement fields u, v, and w. To solve this minimization problem, the Rayleigh-Ritz method can be employed. That consists in finding a set of kinematically admissible displacement field functions which give a good approximation of the displacement fields and satisfy the kinematic and boundary conditions and the compatibility condition given by Eq.(14) in a subspace of the N base functions denoted by h_i $(i = 1, 2, ..., N)$.

$$\frac{\partial^2 \varepsilon^0_{xx}}{\partial y^2} + \frac{\partial^2 \varepsilon^0_{yy}}{\partial x^2} - 2\frac{\partial^2 \varepsilon^0_{xy}}{\partial x \partial y} = 0 \tag{14}$$

A displacement field noted U can be written as

$$U(x, y, z) = \sum_{i=1}^{N} a_i h_i(x, y, z) \tag{15}$$

where a_i are the unknown parameters while h_i are the base functions (such as polynomial and trigonometric functions, Tchebychev polynomials,...). In (Hyer, 1981), Hyer assumes that the out-of-plane displacement field, w, is a quadratic

function of x and y from which he deduces the kinematically admissible in-plane displacement fields, u and v satisfying the condition of compatibility Eq.(14)

$$\begin{cases} u(x,y) = cx - \dfrac{a^2}{6}x^3 - \dfrac{ab}{4}xy^2 \\ v(x,y) = dy - \dfrac{b^2}{6}y^3 - \dfrac{ab}{4}x^2y \\ w(x,y) = \dfrac{1}{2}(ax^2 + by^2) \end{cases} \tag{16}$$

By introducing Eq.(16) into Eq.(4) and Eq.(5), the relations between a, b, c, and d and the components of the in-plane strain tensor and the curvatures of the plate are

$$\begin{cases} \varepsilon^0_{xx} = c - \dfrac{ab}{4}y^2 \\ \varepsilon^0_{yy} = d - \dfrac{ab}{4}x^2 \\ \varepsilon^0_{xy} = 0 \end{cases} \tag{17}$$

and

$$\begin{cases} k_{xx} = a \\ k_{yy} = b \\ k_{xy} = 0 \end{cases} \tag{18}$$

The in-plane strain tensor remains depending on $(x,\ y)$ while in-plane curvature tensor becomes constant. It is necessary to note that the shear strain, ε^0_{xy}, and the shear curvature, k_{xy}, are null. Since the theory predicts ε^0_{xy} and k_{xy} to be zero, the deformed shape of the plate could change from "spherical cap" ($a = b$ and $c = d$) to "concave cylinder" ($a \neq b$ and $c \neq d$) according to the in-plane plate dimensions. The total potential energy depends on a, b, c and d such as

$$E^{tot} = E^{tot}(a, b, c, d)$$

Using Rayleigh-Ritz's approximate fields, the plate can present different shapes under moisture uptake.

By introducing Eq.(17) and Eq.(18) into Eq.(12) and using Eq.(10), E^{tot} can be written as

$$\begin{aligned} E^{tot} = & \frac{1}{2}\int_V Q(m)[(c-\frac{ab}{4}y^2-az)^2+(d-\frac{ab}{4}x^2-bz)^2 \\ & + 2\nu(m)(c-\frac{ab}{4}y^2-az)(d-\frac{ab}{4}x^2-bz)]dV \\ & - \beta\int_V \Delta m Q(m)(1+\nu(m))[(c-\frac{ab}{4}y^2-az)+(d-\frac{ab}{4}x^2-bz)]dV \end{aligned} \tag{19}$$

Integrating $\frac{\partial E^{tot}}{\partial a_i}$ for $i=1,2,3,4$ with $dV=dxdydz$ where $x\in[-\frac{L_x}{2},\ \frac{L_x}{2}]$, $y\in[-\frac{L_y}{2},\ \frac{L_y}{2}]$ and $z\in[-\frac{L_z}{2},\ \frac{L_z}{2}]$, leads to the following equation

$$\begin{aligned} \delta E^{tot} = & f_1^{nl}(a,b,c,d)\delta a + f_2^{nl}(a,b,c,d)\delta b \\ & + f_3^{nl}(a,b,c,d)\delta c + f_4^{nl}(a,b,c,d)\delta d = 0 \end{aligned} \tag{20}$$

where $f_i^{nl}(a,b,c,d),\ i=1,2,3,4$ are non-linear algebric relations between a, b, c and d. Eq.(20) leads to the following non-linear system

$$\begin{cases} f_1^{nl}(a,b,c,d) = a\overline{Q_{cz^2}} + b[\overline{Q^\nu_{cz^2}} + \frac{A_c^\nu(L_x^2+L_y^2)}{48}] - c\overline{Q_{cz}} - d\overline{Q^\nu_{cz}} \\ \qquad + \frac{b^2}{48}(\overline{Q_{cz}}L_x^2 + \overline{Q^\nu_{cz}}L_y^2) + \frac{ab}{24}(\overline{Q_{cz}}L_y^2 + \overline{Q^\nu_{cz}}L_x^2) \\ \qquad - \frac{bc}{48}(\overline{Q_c}L_y^2 + \overline{Q_c^\nu}L_x^2) - \frac{bd}{48}(\overline{Q_c}L_x^2 + \overline{Q_c^\nu}L_y^2) \\ \qquad + ab^2[\frac{\overline{Q_c}(L_x^4+L_y^4)}{1280} + \frac{\overline{Q_c^\nu}L_x^2L_y^2}{1152}] + A^\nu_{cz} = 0 \\ f_2^{nl}(a,b,c,d) = a[\overline{Q^\nu_{cz^2}} + \frac{A_c^\nu(L_x^2+L_y^2)}{48}] + b\overline{Q_{cz^2}} - c\overline{Q^\nu_{cz}} - d\overline{Q_{cz}} \\ \qquad + \frac{a^2}{48}(\overline{Q_{cz}}L_y^2 + \overline{Q^\nu_{cz}}L_x^2) + \frac{ab}{24}(\overline{Q_{cz}}L_x^2 + \overline{Q^\nu_{cz}}L_y^2) \\ \qquad - \frac{ac}{48}(\overline{Q_c}L_y^2 + \overline{Q_c^\nu}L_x^2) - \frac{ad}{48}(\overline{Q_c}L_x^2 + \overline{Q_c^\nu}L_y^2) \\ \qquad + a^2b[\frac{\overline{Q_c}(L_x^4+L_y^4)}{1280} + \frac{\overline{Q_c^\nu}L_x^2L_y^2}{1152}] + A^\nu_{cz} = 0 \\ f_3^{nl}(a,b,c,d) = -a\overline{Q_{cz}} - b\overline{Q^\nu_{cz}} + c\overline{Q_c} + d\overline{Q_c^\nu} - \frac{ab}{48}(\overline{Q_c}L_y^2 + \overline{Q_c^\nu}L_x^2) - A_c^\nu = 0 \\ f_4^{nl}(a,b,c,d) = -a\overline{Q^\nu_{cz}} - b\overline{Q_{cz}} + c\overline{Q_c^\nu} + d\overline{Q_c} - \frac{ab}{48}(\overline{Q_c}L_x^2 + \overline{Q_c^\nu}L_y^2) - A_c^\nu = 0 \end{cases} \tag{21}$$

where

$$\begin{aligned}
\overline{Q_c} &= \frac{1}{L_z}\int_Z Q(m)dz; \quad \overline{Q_c^\nu} = \frac{1}{L_z}\int_Z \nu(m)Q(m)dz \\
\overline{Q_{cz}} &= \frac{1}{L_z}\int_Z Q(m)zdz; \quad \overline{Q_{cz}^\nu} = \frac{1}{L_z}\int_Z \nu(m)Q(m)zdz \\
\overline{Q_{cz^2}} &= \frac{1}{L_z}\int_Z Q(m)z^2dz; \quad \overline{Q_{cz^2}^\nu} = \frac{1}{L_z}\int_Z \nu(m)Q(m)z^2dz \\
A_c^\nu &= \frac{1}{L_z}\int_Z (1+\nu(m))Q(m)\varepsilon_{xx}^H dz; \quad A_{cz}^\nu = \frac{1}{L_z}\int_Z (1+\nu(m))Q(m)\varepsilon_{xx}^H z dz
\end{aligned} \tag{22}$$

Once the in-plane strains and the curvatures are known, the material properties ($\nu(m)$, $E(m)$ and β) given through the integral relations Eq.(22) can be identified.

In experimental mechanics, it is common practice to measure directly the strains and the curvatures, and therefore the vector (a, b, c, d). It can be noticed that the vector (a, b, c, d) depends on time through m, that is $(a, b, c, d) \equiv (a, b, c, d)(t)$. The measured values a, b, c and d are also solutions of the non-linear system Eq.(21). Solving Eq.(21) yields equilibrium positions of the plate which either maximize or minimize the total energy. Being a system of four third-order non-linear equations, Eq.(21) would have either one or three real solutions. With multiple solutions, some of them define a stable equilibrium for which physical interpretation is possible. For stable equilibrium, the total potential energy must be minimized. Thus, for stable equilibrium the second variation of the total potential energy, $\frac{\partial^2 E^{tot}}{\partial a_i \partial a_j}$; $i, j = 1, 2, 3, 4$, must be positive definite (Hyer, 1981). This is true if and only if the following real symmetric matrix is positive definite, (Hyer, 1981)

$$\begin{bmatrix}
\frac{\partial f_1^{nl}}{\partial a} & \frac{\partial f_1^{nl}}{\partial b} & \frac{\partial f_1^{nl}}{\partial c} & \frac{\partial f_1^{nl}}{\partial d} \\
\frac{\partial f_2^{nl}}{\partial a} & \frac{\partial f_2^{nl}}{\partial b} & \frac{\partial f_2^{nl}}{\partial c} & \frac{\partial f_2^{nl}}{\partial d} \\
\frac{\partial f_3^{nl}}{\partial a} & \frac{\partial f_3^{nl}}{\partial b} & \frac{\partial f_3^{nl}}{\partial c} & \frac{\partial f_3^{nl}}{\partial d} \\
\frac{\partial f_4^{nl}}{\partial a} & \frac{\partial f_4^{nl}}{\partial b} & \frac{\partial f_4^{nl}}{\partial c} & \frac{\partial f_4^{nl}}{\partial d}
\end{bmatrix} \tag{23}$$

with

$$
\begin{aligned}
&\frac{\partial f_1^{nl}}{\partial a} = \overline{Q_{cz^2}} + \frac{b}{24}(\overline{Q_{cz}}L_y^2 + \overline{Q_{cz}^{\nu}}L_x^2) + b^2[\frac{\overline{Q_c}(L_x^4 + L_y^4)}{1280} + \frac{\overline{Q_c^{\nu}}L_x^2 L_y^2}{1152}] \\
&\frac{\partial f_1^{nl}}{\partial b} = \frac{\partial f_2^{nl}}{\partial a} = \overline{Q_{cz^2}^{\nu}} + \frac{(L_x^2 + L_y^2)A_c^{\nu}}{48} + \frac{b}{24}(\overline{Q_{cz}}L_x^2 + \overline{Q_{cz}^{\nu}}L_y^2) + \frac{a}{24}(\overline{Q_{cz}}L_y^2 + \overline{Q_{cz}^{\nu}}L_x^2) \\
&\qquad - \frac{c}{48}(\overline{Q_c}L_y^2 + \overline{Q_c^{\nu}}L_x^2) - \frac{d}{48}(\overline{Q_c}L_x^2 + \overline{Q_c^{\nu}}L_y^2) + ab[\frac{\overline{Q_c}(L_x^4 + L_y^4)}{640} + \frac{\overline{Q_c^{\nu}}L_x^2 L_y^2}{576}] \\
&\frac{\partial f_1^{nl}}{\partial c} = \frac{\partial f_3^{nl}}{\partial a} = -\overline{Q_{cz}} - \frac{b}{48}(\overline{Q_c}L_y^2 + \overline{Q_c^{\nu}}L_x^2) \\
&\frac{\partial f_1^{nl}}{\partial d} = \frac{\partial f_4^{nl}}{\partial a} = -\overline{Q_{cz}^{\nu}} - \frac{b}{48}(\overline{Q_c}L_x^2 + \overline{Q_c^{\nu}}L_y^2) \\
&\frac{\partial f_2^{nl}}{\partial b} = \overline{Q_{cz^2}} + \frac{a}{24}(\overline{Q_{cz}}L_x^2 + \overline{Q_{cz}^{\nu}}L_y^2) + a^2[\frac{\overline{Q_c}(L_x^4 + L_y^4)}{1280} + \frac{\overline{Q_c^{\nu}}L_x^2 L_y^2}{1152}] \\
&\frac{\partial f_2^{nl}}{\partial c} = \frac{\partial f_3^{nl}}{\partial b} = -\overline{Q_{cz}^{\nu}} - \frac{a}{48}(\overline{Q_c}L_y^2 + \overline{Q_c^{\nu}}L_x^2) \\
&\frac{\partial f_2^{nl}}{\partial d} = \frac{\partial f_4^{nl}}{\partial b} = -\overline{Q_{cz}} - \frac{a}{48}(\overline{Q_c}L_x^2 + \overline{Q_c^{\nu}}L_y^2) \\
&\frac{\partial f_3^{nl}}{\partial c} = \overline{Q_c};\ \frac{\partial f_3^{nl}}{\partial d} = \frac{\partial f_4^{nl}}{\partial c} = \overline{Q_c^{\nu}};\ \frac{\partial f_4^{nl}}{\partial d} = \overline{Q_c}
\end{aligned}
\tag{24}
$$

Before illustrating the different solutions (shapes) that can be obtained, the particular case of the geometrically linear approach is detailed. In the geometrically linear theory, the problem (21) takes a simple form. In fact, the linear problem is obtained by neglecting non-linear terms $(\frac{\partial w}{\partial x})^2$, $(\frac{\partial w}{\partial y})^2$ and $(\frac{\partial w}{\partial x})(\frac{\partial w}{\partial y})$ in the strain tensor (Eq.(4)) yielding to its reduced expression (Eq.(25))

$$
\mathbf{E}^0 = \begin{cases} \varepsilon_{xx}^0 = \dfrac{\partial u}{\partial x} \\ \varepsilon_{yy}^0 = \dfrac{\partial v}{\partial y} \\ 2\varepsilon_{xy}^0 = \dfrac{\partial u}{\partial y} + \dfrac{\partial v}{\partial x} \end{cases} \tag{25}
$$

In this case, the chosen in-plane displacement fields u and v are linear functions of x and y respectively while the out-of-plane displacement field w is quadratic in x and y (Hyer, 1981; Gigliotti and Minervino, 2014)

$$
\begin{cases} u(x,y) = cx \\ v(x,y) = dy \\ w(x,y) = \dfrac{1}{2}(ax^2 + by^2) \end{cases} \tag{26}
$$

Thus, the relations between a, b, c and d and the components of the in-plane strain tensor and curvatures of the plate are

$$\begin{cases} \varepsilon^0_{xx} = c \\ \varepsilon^0_{yy} = d \\ \varepsilon^0_{xy} = 0 \end{cases} \qquad (27) \qquad \begin{cases} k_{xx} = a \\ k_{yy} = b \\ k_{xy} = 0 \end{cases}$$

It can be seen that the geometrically linear theory leads to constant strain (Eq.(27)) with the same constant curvature tensor. Due to moisture uptake, the deformed shape of the plate will be like spherical cap whatever the plate in-plane dimension.

The first variation of the total potential energy (first equation of Eq.(13)) can be written as

$$\begin{aligned} \delta E^{tot} = & f^l_1(a,b,c,d)\delta a + f^l_2(a,b,c,d)\delta b \\ & + f^l_3(a,b,c,d)\delta c + f^l_4(a,b,c,d)\delta d = 0 \end{aligned} \qquad (28)$$

immediatly leading up to the following system of four linear equations in a, b, c and d

$$\begin{cases} f^l_1(a,b,c,d) = -a\overline{Q_{cz}} - b\overline{Q^\nu_{cz}} + c\overline{Q_c} + d\overline{Q^\nu_c} - A^\nu_c = 0 \\ f^l_2(a,b,c,d) = -a\overline{Q^\nu_{cz}} - b\overline{Q_{cz}} + c\overline{Q^\nu_c} + d\overline{Q_c} - A^\nu_c = 0 \\ f^l_3(a,b,c,d) = -a\overline{Q_{cz^2}} - b\overline{Q^\nu_{cz^2}} + c\overline{Q_{cz}} + d\overline{Q^\nu_{cz}} - A^\nu_{cz} = 0 \\ f^l_4(a,b,c,d) = -a\overline{Q^\nu_{cz^2}} - b\overline{Q_{cz^2}} + c\overline{Q^\nu_{cz}} + d\overline{Q_{cz}} - A^\nu_{cz} = 0 \end{cases} \qquad (29)$$

Eq.(29) can be written under matrix system as follows

$$\begin{bmatrix} -\overline{Q_{cz}} & -\overline{Q^\nu_{cz}} & \overline{Q_c} & \overline{Q^\nu_c} \\ -\overline{Q^\nu_{cz}} & -\overline{Q_{cz}} & \overline{Q^\nu_c} & \overline{Q_c} \\ -\overline{Q_{cz^2}} & -\overline{Q^\nu_{cz2}} & \overline{Q_{cz}} & \overline{Q^\nu_{cz}} \\ -\overline{Q^\nu_{cz^2}} & -\overline{Q_{cz^2}} & \overline{Q^\nu_{cz}} & \overline{Q_{cz}} \end{bmatrix} \begin{pmatrix} a \\ b \\ c \\ d \end{pmatrix} = \begin{pmatrix} A^\nu_c \\ A^\nu_c \\ A^\nu_{cz} \\ A^\nu_{cz} \end{pmatrix} \qquad (30)$$

Eq.(29) (or Eq.(30)) is a system of four first-order equations in terms of a, b, c

and d. Such a problem would have unique real solution written in Eq.(31)

$$\begin{cases} a = b = \dfrac{(\overline{Q_c} + \overline{Q_c^\nu})A_{cz}^\nu - (\overline{Q_{cz}} + \overline{Q_{cz}^\nu})A_c^\nu}{(\overline{Q_{cz}} + \overline{Q_{cz}^\nu})^2 - (\overline{Q_c} + \overline{Q_c^\nu})(\overline{Q_{cz^2}} + \overline{Q_{cz^2}^\nu})} \\ c = d = \dfrac{(\overline{Q_{cz^2}} + \overline{Q_{cz^2}^\nu})A_c^\nu - (\overline{Q_{cz}} + \overline{Q_{cz}^\nu})A_{cz}^\nu}{(\overline{Q_{cz^2}} + \overline{Q_{cz^2}^\nu})(\overline{Q_c} + \overline{Q_c^\nu}) - (\overline{Q_{cz}} + \overline{Q_{cz}^\nu})^2} \end{cases} \tag{31}$$

Moreover, longitudinal and transversal strains are equal ($a = b$) as well as longitudinal and transversal curvatures ($c = d$).

$$a = b \text{ and } c = d \tag{32}$$

The unique solution Eq.(31) defines stable equilibrium position if the following matrix is positive definite

$$\begin{bmatrix} \frac{\partial f_1^l}{\partial a} & \frac{\partial f_1^l}{\partial b} & \frac{\partial f_1^l}{\partial c} & \frac{\partial f_1^l}{\partial d} \\ \frac{\partial f_2^l}{\partial a} & \frac{\partial f_2^l}{\partial b} & \frac{\partial f_2^l}{\partial c} & \frac{\partial f_2^l}{\partial d} \\ \frac{\partial f_3^l}{\partial a} & \frac{\partial f_3^l}{\partial b} & \frac{\partial f_3^l}{\partial c} & \frac{\partial f_3^l}{\partial d} \\ \frac{\partial f_4^l}{\partial a} & \frac{\partial f_4^l}{\partial b} & \frac{\partial f_4^l}{\partial c} & \frac{\partial f_4^l}{\partial d} \end{bmatrix} = \begin{bmatrix} -\overline{Q_{cz}} & -\overline{Q_{cz}^\nu} & \overline{Q_c} & \overline{Q_c^\nu} \\ -\overline{Q_{cz}^\nu} & -\overline{Q_{cz}} & \overline{Q_c^\nu} & \overline{Q_c} \\ -\overline{Q_{cz^2}} & -\overline{Q_{cz2}^\nu} & \overline{Q_{cz}} & \overline{Q_{cz}^\nu} \\ -\overline{Q_{cz^2}^\nu} & -\overline{Q_{cz^2}} & \overline{Q_{cz}^\nu} & \overline{Q_{cz}} \end{bmatrix} \tag{33}$$

Since single-valued solution is get in the geometrically linear case, stable equilibrium solution is defined.

3. Illustration of the direct problem

The direct problem is obtained when the mechanical properties $\nu(m)$, $E(m)$ and β are known while the vector (a, b, c, d) is the only unknown of Eq.(21). The study of the direct problem is carried out here to illustrate the different shapes that can be obtained for characteristic parameter values of the RTM6 resin for several aspect ratios of a square plate in the geometrically linear and non-linear cases. To study strain and curvature evolutions, numerical simulations are performed with diffuso-mechanical RTM6 resin properties listed in Tab.1. The Young's modulus depends linearly on moisture content, m as experimentally noted (Simar, 2014). The simulations concern a plate with thickness of L_z equal to 4mm. The diffusion equation, Eq.(1) has been solved with the

Table 1: RTM6 resin properties

E(m)(GPa)	ν	$D_{zz}(\text{mm}^2.\text{h}^{-1})$	β	$m^2_\infty(\%)$	$m^1_\infty(\%)$
$-20,46\text{m}+3,14$	$0,35$	$0,016$	$0,22$	$3,1\%$	$0,4m^2_\infty$

finite difference method. Figures 2 and 3 illustrate the fields m and $E(m)$ along the thickness z direction of the plate, for different times up to saturation. Having different moisture concentrations on the two opposite surfaces of the plate leads to asymmetric boundary conditions and asymmetric distributions of m and $E(m)$ as depicted in Fig.2 and Fig.3. The evolution of the moisture content average ($\overline{m}$) with time is illustrated in Fig.4. For a given equilibrium solution in a given time, the matrix as in Eq.(23) and Eq.(33) in the particular case of the geometrically linear approach is numerically evaluated. If each of their eigenvalues is positive, the matrix is positive definite and then the solution matches to a stable equilibrium solution. Otherwise the solution corresponds to an unstable equilibrium solution. For diffuso-mechanical properties given for RTM6 resin and listed in Tab.1 with a fixed thickness length ($L_z = 4\text{mm}$), triple-valued solutions could be observed for Eq.(21) according to the in-plane plate dimension. Thus, for a square plate of aspect ratio less than 60 ($AR_{xz} = AR_{yz} = \frac{L_x}{L_z} < 60$), Eq.(21) and obviously Eq.(30) lead to a single-valued solution. Figures 5 and 6 illustrate the evolutions of the strains and the curvatures for $AR_{xz} = AR_{yz} = \frac{L_x}{L_z} = 10$. The solutions in the two approaches (geometrically linear and non-linear) are very close. In these conditions, the deformed shape of the plate is like a spherical cap as schematically illustrated in Fig.7.

However, for a higher aspect ratio ($AR_{xz} \geq 60$), triple-valued solutions are found from a critical point for the general problem while the geometrically linear approach always presents a single-valued solution. It is shown in Fig.8 and Fig.9 that the solutions in linear and non-linear approaches are widely different for $AR_{xz} = AR_{yz} = 100$.

Since single-valued solution is obtained before the critical point (branch AB

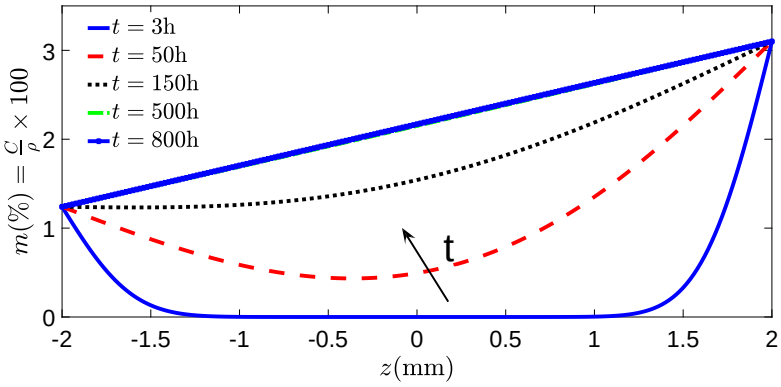

Figure 2: Evolution of the current moisture content m along the thickness z for different times

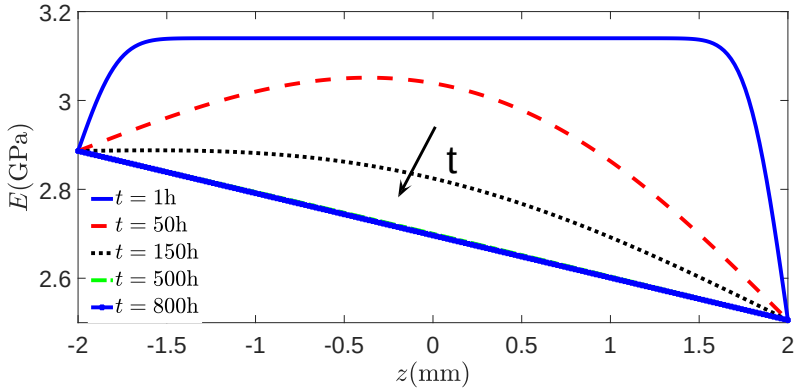

Figure 3: Evolution of the Young's modulus $E(m)$ along the thickness z for different times, m being the current moisture content

in the Fig.8), it defines stable equilibrium position of the plate. Moreover, on the branch AB and on the branch BD after the critical point, the condition Eq.(32) is satisfied as in the geometrically linear approach. Furthermore, after the critical point, only branch BD was unstable while branches BC and BE were stable. Moreover, branch BE defines a significant curvature in the x direction while branch BC represents a curvature in the y direction which tends asymptotically to zero. This corresponds to a "concave cylinder" of axis y as

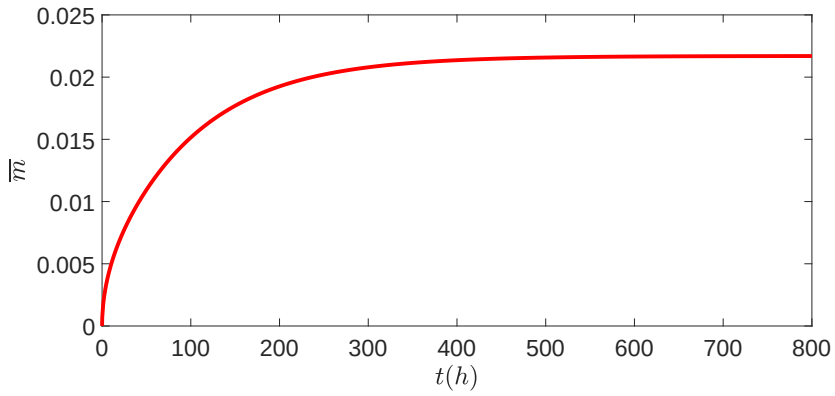

Figure 4: Evolution of the average of the current moisture content, $\overline{m}$, with respect to time t

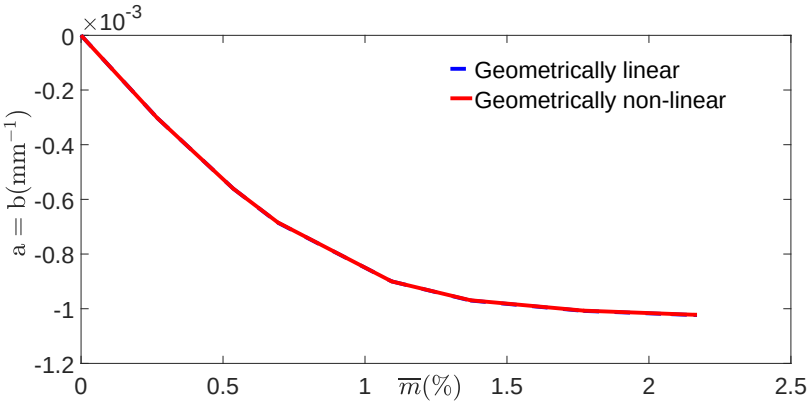

Figure 5: Evolution of in-plane curvatures (a and b) in geometrically linear and non-linear approaches for aspect ratios $AR_{xz} = AR_{yz} = 10$

schematically depicted in Fig.10. In the y direction, the branch BE corresponds to the branch BC and vice-versa. It is necessary to note that triple-valued solutions can be also obtained for a rectangular plate ($AR_{xz} > AR_{yz}$) as schematically illustrated in Fig.11. However, the solutions in c (Fig.12) and d (Fig.13) before the critical point may be different.

The triple-valued type of solutions shows that in the explored interval of $\overline{m}$, hygroscopic "loading" can lead to change the plate shapes from spherical cap to cylinder with respect to geometrical defects. This leads to a limitation for the

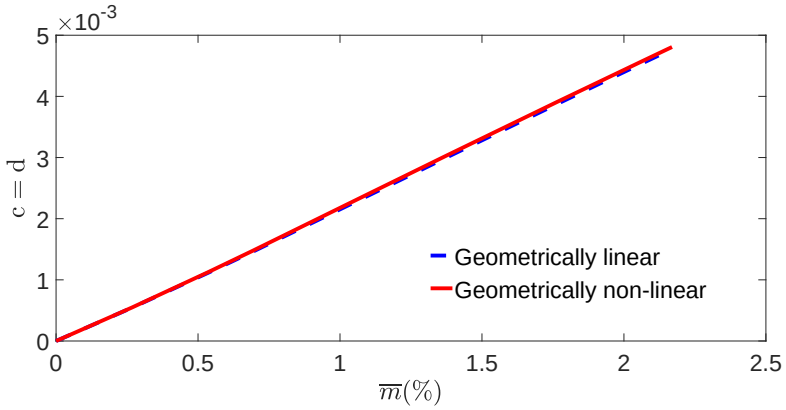

Figure 6: Evolution of in-plane strains (c and d) in geometrically linear and non-linear approaches for aspect ratios $AR_{xz} = AR_{yz} = 10$

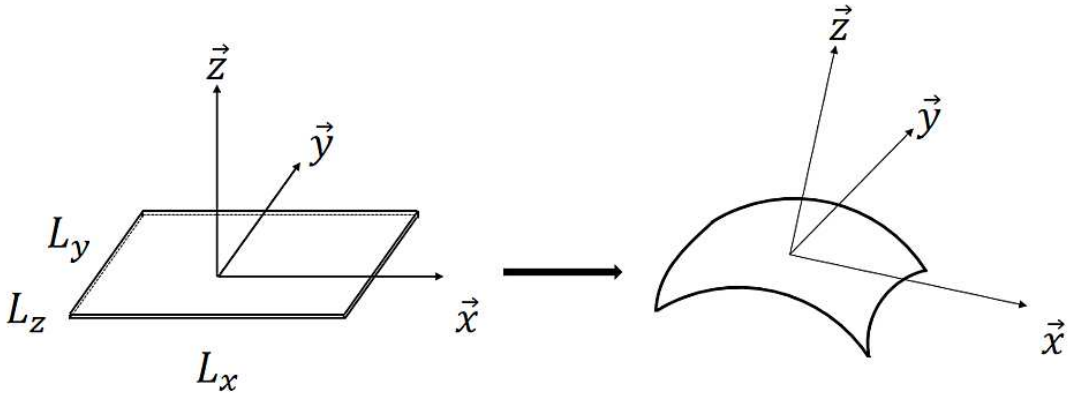

Figure 7: In the geometrically linear approach, the plate deforms to a spherical cap

identification after the critical point due to the multiplicity of solutions. Triple-valued solutions are obtained also in terms of strains (c and d) with $c \neq d$ but stay in the same order of magnitude. The condition (32) is satisfied either in the geometrically linear case or before the critical point if triple-value solutions occur in the geometrically non-linear approach. To this end (and because of the use of square plate), the first two equations of Eq.(21) are the same as well as the last two equations. In this study, the identification is performed only for this particular situation that leads to the uniqueness of the solution.

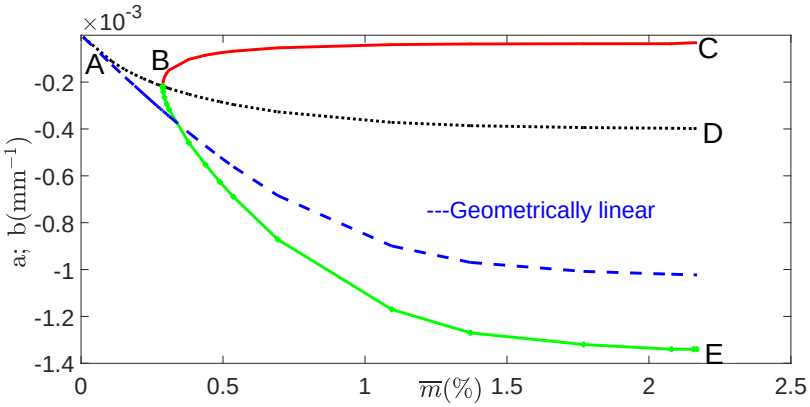

Figure 8: Evolution of in-plane curvatures (a and b) in geometrically linear and non-linear approaches for aspect ratios $AR_{xz} = AR_{yz} = 100$

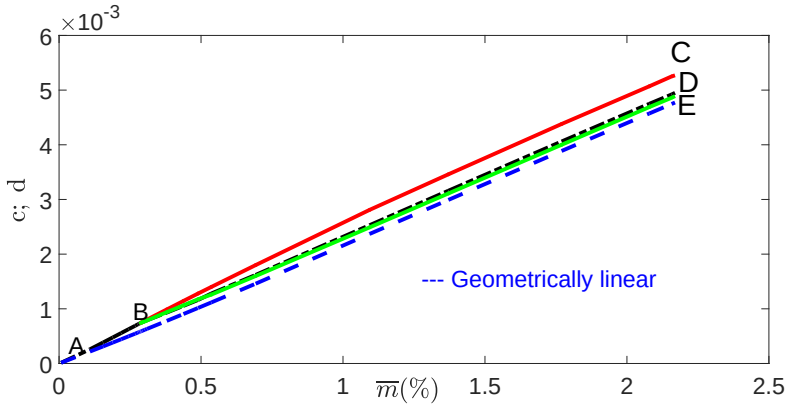

Figure 9: Evolution of in-plane strains (c and d) in geometrically linear and non-linear approaches for aspect ratios $AR_{xz} = AR_{yz} = 100$

The different responses of the material in terms of in-plane strains and curvatures being well illustrated, the identification in geometrically linear and non-linear approaches of diffuso-mechanical properties ($\nu(m)$, $E(m)$ and β) is performed in section 4.

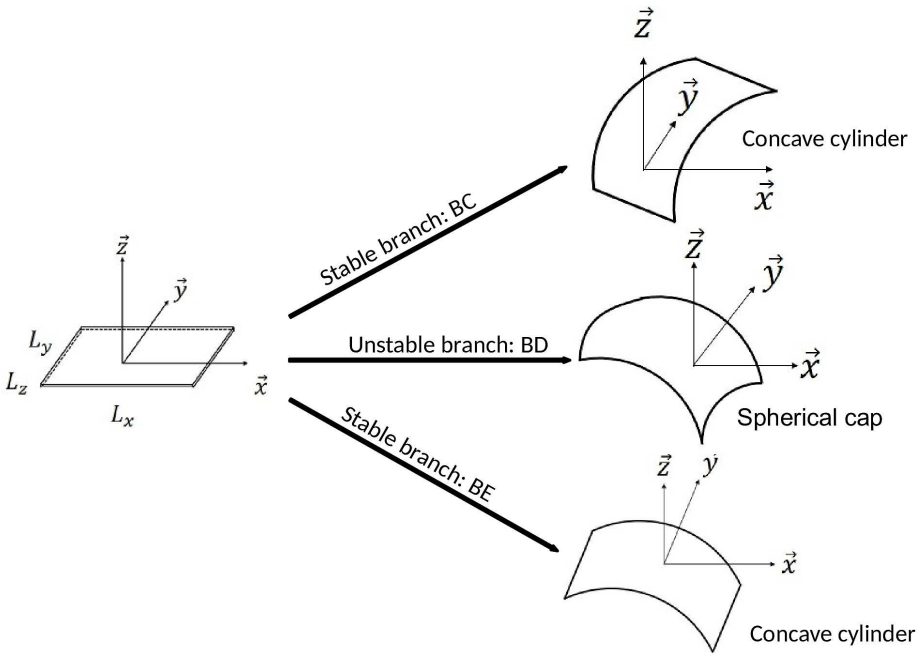

Figure 10: Plate deformed shape in the geometrically non-linear approach with a triple-valued solution in term of strains and curvatures after the critical point

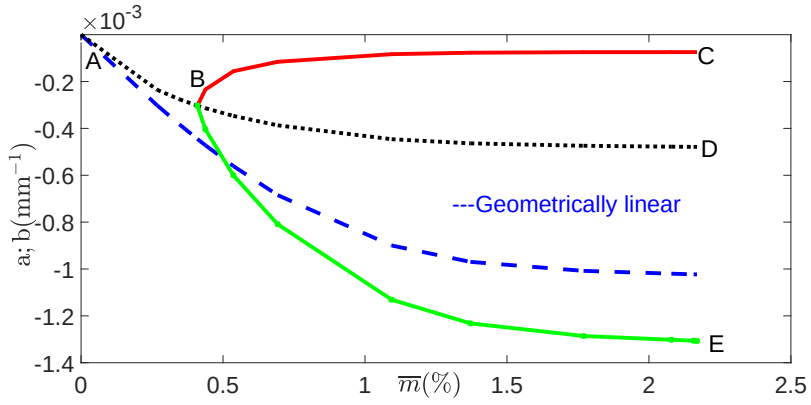

Figure 11: Evolution of the in-plane curvatures (a and b) in geometrically linear and non-linear approaches for aspect ratios $AR_{xz} = 100$ and $AR_{yz} = 10$

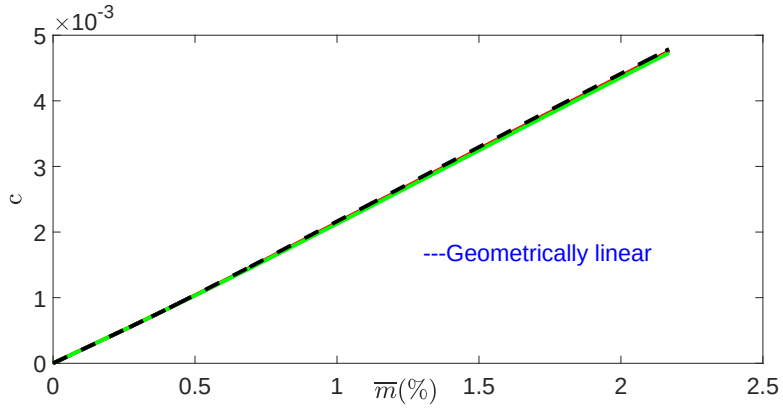

Figure 12: Evolution of the in-plane strains (c) in geometrically linear and non-linear approaches for aspect ratios $AR_{xz} = 100$ and $AR_{yz} = 10$

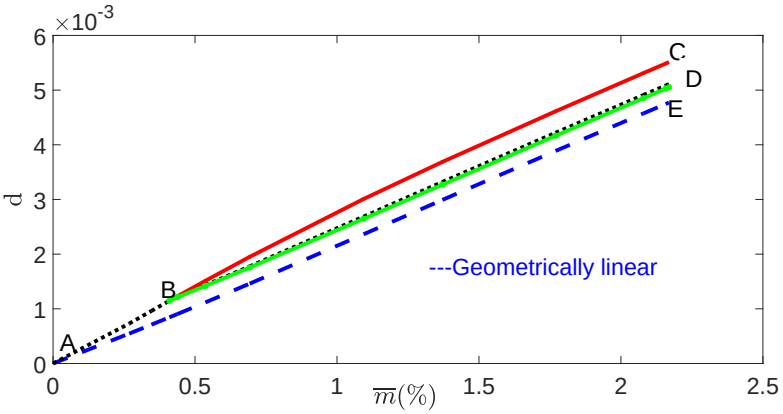

Figure 13: Evolution of the in-plane strains (d) in geometrically linear and non-linear approaches for aspect ratios $AR_{xz} = 100$ and $AR_{yz} = 10$

4. Identification

The identification consists in calculating the elastic diffuso-mechanical properties, $\nu(m)$, $E(m)$ and β when vector (a, b, c, d) is assumed to be experimentally measured. It involves to solve inverse problems in Eq.(30) and Eq.(21). In this part, as mentioned in section 3, our study is restricted to the geometrically non-linear case before bifurcation so that the identification is conducted on a problem with a single solution. For this purpose, the study is made for partic-

ular plate aspect ratios and for particular moisture uptakes or particular times. The Poisson's ratio $\nu(m)$ and the coefficient of moisture expansion β are assumed to be independent of moisture content ($\nu(m) = \nu$). The identification is illustrated for two profiles of Young's modulus related to m :

- E is independent of moisture content: $E(m) = E$
- $E(m)$ is a linear function of m : $E(m) = \alpha m + \eta$

4.1. Identification in the geometrically linear approach

4.1.1. E is independent of m

Since ν and β are constant, the independence of E on moisture content leads to the system Eq.(34) in which ν and E are missing.

$$\begin{cases} c = d = \beta\overline{m} \\ a = b = -\dfrac{12\beta\overline{mz}}{L_z^2} \end{cases} \tag{34}$$

Therefore, only the coefficient of moisture expansion, β, can be identified. Eq.(35) shows that β can be expressed in two ways

$$\begin{cases} \beta_1 = \dfrac{c}{\overline{m}} \\ \beta_2 = -\dfrac{aL_z^2}{12\overline{mz}} \end{cases} \tag{35}$$

4.1.2. E(m) is a linear function of m

In the case $E(m)$ is a linear function of m, $E(m) = \alpha m + \eta$, Eq.(31) becomes

$$\begin{cases} (\alpha\overline{m} + \eta)c - \alpha\overline{mz}a = \beta(\alpha\overline{m^2} + \eta\overline{m}) \\ \alpha\overline{mz}c - (\alpha\overline{mz^2} + \dfrac{\eta L_z^2}{12})a = \beta(\alpha\overline{m^2 z} + \eta\overline{mz}) \end{cases} \tag{36}$$

where

$$\overline{m^2} = \frac{1}{L_z}\int_Z m^2 dz; \quad \overline{mz^2} = \frac{1}{L_z}\int_Z mz^2 dz \text{ and } \overline{m^2 z} = \frac{1}{L_z}\int_Z m^2 z dz$$

One finds that only ν is missing in Eq.(36), so it can not be identified. 3 parameters, α, η and β should be identified with the system Eq.(36) of 2 equations.

But since η is the value of Young's modulus before moisture uptaking, it can be identified on a dry sample by adding another test (tensile or bending test on dry sample) to the asymmetric one. By expressing α from the first equation of Eq.(36) and introducing it in the second equation, we have

$$\begin{cases} h_1\beta^2 + h_2\beta + h_3 = 0 \\ \alpha = \dfrac{(\beta\overline{m} - c)\eta}{\overline{m}c - \overline{mz}a - \beta\overline{m^2}} \end{cases} \tag{37}$$

where

$$\begin{aligned} h_1 &= \overline{m^2}\,\overline{mz} - \overline{m^2 z}\,\overline{m} \\ h_2 &= c\overline{m^2 z} + a\frac{\overline{m^2}L_z^2}{12} + (c\overline{mz} - a\overline{mz^2})\overline{m} - (c\overline{m} - a\overline{mz})\overline{mz} \\ h_3 &= -c(c\overline{mz} - a\overline{mz^2}) - a(c\overline{m} - a\overline{mz})\frac{L_z^2}{12} \end{aligned}$$

2 values of β can be obtained from the first equation of Eq.(37) if the following condition is satisfied

$$h_2^2 - 4h_1h_3 \geq 0 \tag{38}$$

The best solution will be one of both solutions which is constant (as assumed) and will then be used to identify α.

It can be noticed that η is known before the moisture stated diffusing in the material. So its value can be used to determine β and α.

4.2. Identification in the geometrically non-linear approach

In the geometrically non-linear approach, the identification is complicated due to the presence of multiple branches. If triple-valued solutions occur, the condition (32) is satisfied only before the critical point. To this end (and because of the use of square plate), the first two equations of Eq.(21) are the same as well as the last two equations. In the geometrically non-linear approach, the identification is performed only for this particular situation.

4.2.1. E is independent of m

In the case $E(m) = E$, β can be directly expressed from Eq.(21) as in Eq.(39) while ν is expressed by Eq.(40) using β

$$\beta = \frac{48c - a^2 L_x^2}{48\overline{m}} \tag{39}$$

$$\nu = (\frac{1152}{640})\frac{640A_\beta - a^3 L_x^4}{a^3 L_x^4 - 1152A_\beta} \tag{40}$$

where

$$A_\beta = \frac{acL_x^2}{24} - \frac{a}{24}(2L_z^2 + \beta\overline{m}L_x^2) - \beta\overline{mz} \tag{41}$$

It can be noted that E is not determined. Other tests (tensile or bending test) on a dry sample would be employed for identification of E.

4.2.2. $E(m)$ is a linear function of m

Under linear dependence of E with respect to m, 4 parameters ν, α, η and β have to be identified. The system Eq.(21) being reduced to two non-linear equations, Eq.(42), only two parameters (α and β) can be identified by assuming that ν and η are determined on dry sample with tensile or bending test. β and α are then identified by solving 2 non-linear equations, Eq.(42)

$$\begin{cases} a(B_{cz^2} + \frac{A_c L_x^2}{24}) - cB_{cz} + \frac{3a^2 L_x^2 B_{cz}}{48} - \frac{acL_x^2 B_c}{24} + \frac{(1152 + 640\nu)a^3 L_x^4 B_c}{640 \times 1152(1+\nu)} + A_{cz} = 0 \\ aB_{cz} - cB_c + \frac{a^2 L_x^2 B_c}{48} + A_c = 0 \end{cases} \tag{42}$$

where

$$\begin{aligned} B_c &= \frac{1}{L_z}\int_Z E(m)dz = \alpha\overline{m} + \eta \\ B_{cz} &= \frac{1}{L_z}\int_Z E(m)zdz = \alpha\overline{mz} \\ B_{cz^2} &= \frac{1}{L_z}\int_Z E(m)z^2dz = \alpha\overline{mz^2} + \frac{\eta L_z^2}{12} \\ A_c &= \frac{\beta}{L_z}\int_Z E(m)mdz = \beta(\alpha\overline{m^2} + \eta\overline{m}) \\ A_{cz} &= \frac{\beta}{L_z}\int_Z E(m)mzdz = \beta(\alpha\overline{m^2 z} + \eta\overline{mz}) \end{aligned} \tag{43}$$

5. Numerical results for identification

All numerical simulations are carried out with diffuso-mechanical properties given in Tab.1 for RTM6 resin with a fixed thickness $L_z = 4$mm. The equation diffusion Eq.(1) has been solved with the finite difference method using Matlab software leading to the determination of the moisture content, m. When Young's modulus is a linear function of m, it is expressed by

$$E(m) = \alpha m + \eta \tag{44}$$

as experimentally measured in (Simar, 2014) for a RTM6 resin material. When E (independent of m) or η and ν are assumed to be identified on a dry sample, $E = 3.14$GPa, $\nu = 0.35$ and $\eta = 3.14$GPa.

5.1. Geometrically linear approach

5.1.1. E is independent of m

Only the coefficient of moisture expansion is identified with two expressions β_1 and β_2 in Eq.(35). Figure 14 illustrates the evolutions of β_1 and β_2 with respect to times and shows that $\beta_1 = \beta_2$ for all time.

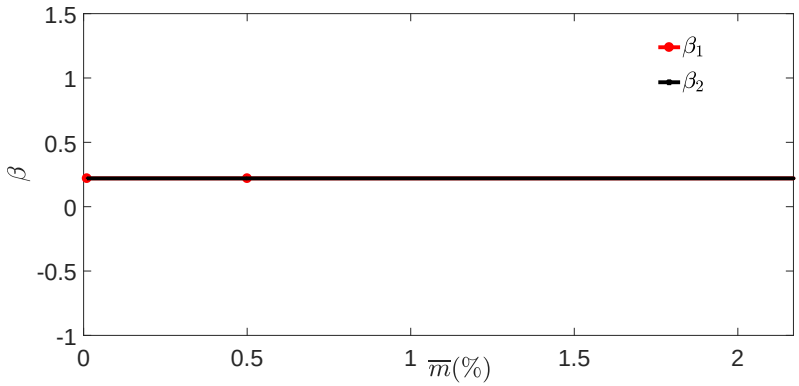

Figure 14: Identified value of the coefficient of moisture expansion β in the geometrically linear approach with the Young's modulus $E(m) = E$

5.1.2. E is a linear function of m

Fig.15 and Fig.16 illustrate the evolutions of the identified parameters β and α respectively with respect to time. Two solutions of β, β_1 and β_2, are obtained. β_1 (solid line) is independent of time and equal to 0.22 (the target values of β) with quadratique error of 10^{-13}. β_2 (dash line) increases with respect to time and converges to 0.22 from a given time. It makes sense to say that the constant solution (β_1) is the best one because β is assumed to be independent of m.

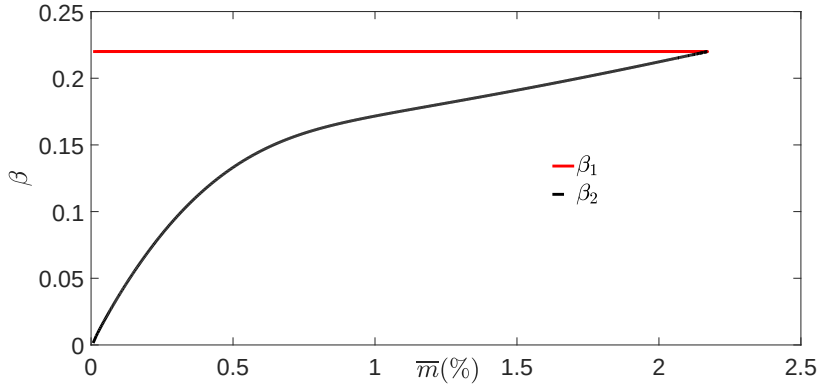

Figure 15: Identified value of the coefficient of moisture expansion β in the geometrically linear approach when the Young's modulus $E(m)$ is a linear function of the current moisture content m

5.2. Geometrically non-linear approach

5.2.1. E is independent of m

In this case, β and ν were identified and were very close to their target values ($\nu \simeq 0.35$ and $\beta \simeq 0.22$) for all time as illustrated in Fig.17 and Fig.18.

5.2.2. E is a linear function of m

When $E(m)$ is a linear function of m (Eq.(44)), β and α were identified by solving with Matlab software the system of two non-linear equations, Eq.(42). Two solutions were found for every parameters: β_1 and β_2 for parameter β and α_1 and α_2 for parameter α as depicted in Fig.19 and Fig.20. β_1 and α_1 are

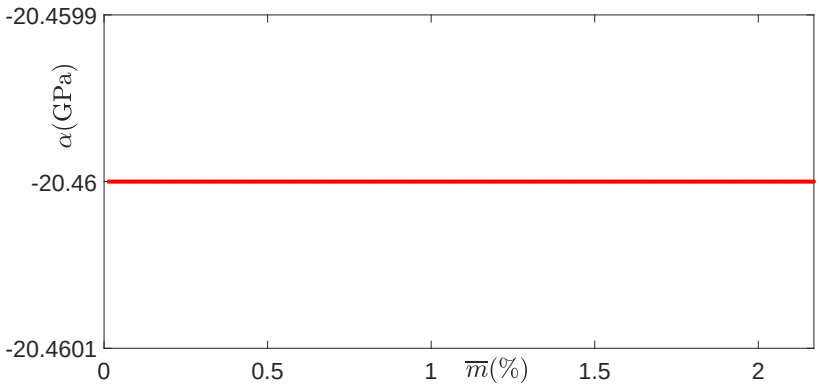

Figure 16: Identified α value in the geometrically linear approach when the Young's modulus $E(m)$ is a linear function of the current moisture content m such as $E(m) = \alpha m + \eta$

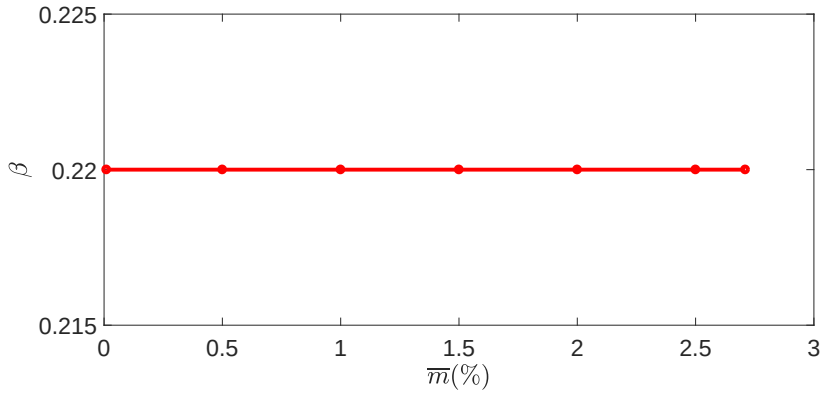

Figure 17: Identified value of the coefficient of moisture expansion β in the geometrically non-linear approach before critical point when the Young's modulus $E(m) = E$

independent of m up to critical point and are equal to their target values, 0.22 and -20.46GPa respectively. The second solution for β (β_2) and α (α_2) increases and decreases respectively with respect to $\overline{m}$. Constant solutions, β_1 and α_1 are the appropriate solutions because they are assumed to be independent of m. Fig.21 is a zoom on α_1 in order to show correctly its constant value, (-20.46GPa) in Fig.20.

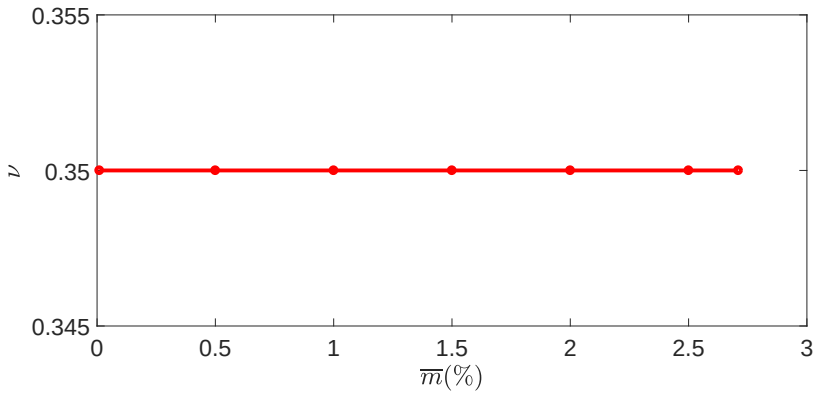

Figure 18: Identified value of the Poisson's ratio ν in the geometrically non-linear approach before critical point when the Young's modulus $E(m) = E$

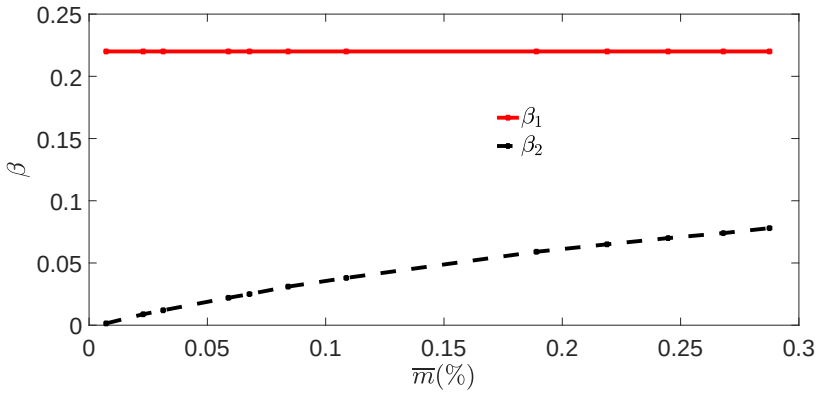

Figure 19: Identified value the coefficient of moisture expansion β in the geometrically non-linear approach before the critical point when the Young's modulus $E(m)$ is a linear function of the current moisture content m

6. Discussion

Although the identification after the critical point was not explored, the results of this study are very promising. Indeed, the study has allowed simultaneous identification of diffuso-mechanical properties with the coefficient of moisture expansion, whereas many authors devoted their studies to the identification of either hygroelastic mechanical properties or the coefficient of moisture

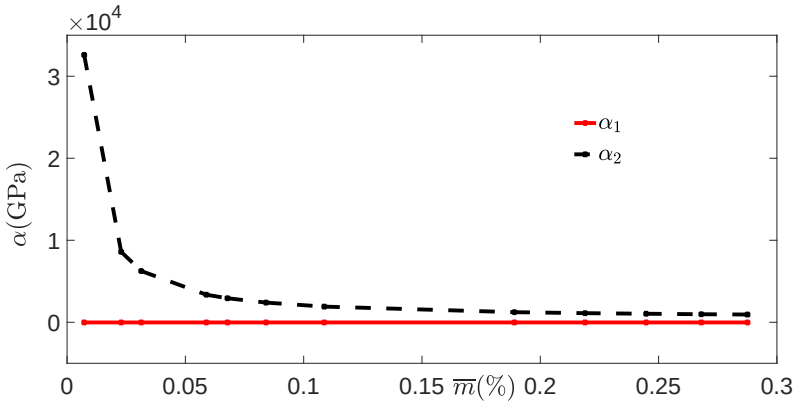

Figure 20: Identified α values in the geometrically non-linear approach before the critical point when the Young's modulus $E(m)$ is a linear function of the current moisture content m such as $E(m) = \alpha m + \eta$

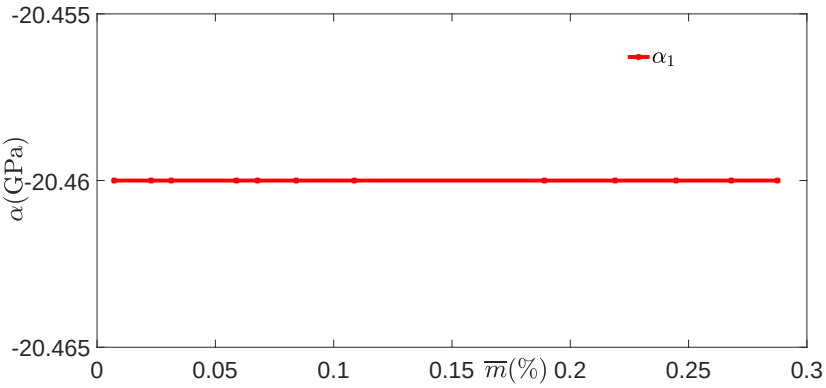

Figure 21: Zoom on the identified α value in the geometrically non-linear approach before the critical point when the Young's modulus $E(m)$ is a linear function of the current moisture content m such as $E(m) = \alpha m + \eta$

expansion (Simar, 2014; Simar et al., 2014; Obeid et al., 2018). Moreover, our study is based on the use of asymmetric concentration fields to perform identification on samples with moisture gradients while in the literature, identification studies were conducted using mechanical tests (tensile test especially) on saturated moisture samples (Simar, 2014; Simar et al., 2014). The advantage of the test based on the use of a sample with moisture gradients is that the identifi-

cation was performed in a transient state, so the conditioning time was shorter than that for saturated samples as already illustrated in our previous article (Djato et al., 2018). For the direct problem, expected results were observed. Indeed, the evolutions of a, b, c and d quantities in the geometrically non-linear approach can present two stable and one unstable equilibrium solutions from a critical point according to the in-plane plate dimension. The figures showed that these solutions promote deflection of the plate from "spherical cap" shape to "concave cylinder" shape, a phenomenon observed by many researchers (Hyer, 1981).

Whereas direct problem presents expected results, the multiplicity of solutions makes the identification difficult, especially after the critical point. The results of the identification are illustrated on RTM6 resin square sample for a constant Young's modulus and then for a linear Young's modulus related to moisture content while Poisson's ratio and the coefficient of moisture expansion are assumed to be independent of moisture content. In the geometrically linear case and for the branch before the critical point in the geometrically non-linear approach, β was identified while $E(m) = E$ could not be identified. Besides, α was only identified when $E(m) = \alpha m + \eta$ whereas $\nu(m) = \nu$ was identified only for the geometrically non-linear case when $E(m) = E$. The identification of η was not possible with the use of the asymmetric concentration field. However, by associating other mechanical tests (tensile, bending,...) on a dry sample, all unidentified parameters for a specific dependence in this study can be identified.

7. Conclusion and perspectives

The present study was devoted to the possibility of the identification of diffuso-mechanical properties and in particular the coefficient of moisture expansion through numerical simulation for polymer matrix material with original test which makes use of plate with asymmetric moisture concentration field. The study is based on a weakly coupled diffuso-mechanical model: 1D Fick's diffusion model solved by finite difference method and 2D plane stress hygroelastic

thin plate model associated with Rayleigh-Ritz method in geometrically linear and non-linear approaches. The direct problem providing the in-plane stresses and the in-plane curvatures led to single-valued or triple-valued solutions up to a critical point for the average of the moisture content for the geometrically non-linear approach according to the in-plane plate dimensions. However, an only single-valued solution was always obtained whatever the plate configuration in the geometrically linear case. The study leads to the identification of β contrary to our previous work, (Djato et al., 2018), based on the use of tensile and/or bending tests for rapid identification of the mechanical properties of polymer matrix materials with moisture gradients in which the experimental measurements (in-plane residual strains and curvatures) depend on β. The identification was here carried out by considering that β and ν are constant parameters while two assumptions for E on its dependence on moisture content were postulated: E is independent of m and $E(m)$ is a linear function of m. For the case E is independent of m, only β was identified in the geometrically linear approach. Two analytical expressions of β were then obtained from in-plane strains and in-plane curvatures respectively. However, both expressions were numerically equal. Besides, in the geometrically non-linear approach, β and ν were identified when $E(m) = E$. α is identified when $E(m) = \alpha m + \eta$. Thus, β and α were determined in geometrically linear and non-linear approaches. Moreover, β and α yield 2 values for each parameter: one is constant and other is a function of m. However, from a given time point, the two resulting values for each parameter became equal in the geometrically linear approach. A parameter (ν or E or η), that could not be identified in the studied case, was considered as determined on a dry sample by associating another test as tensile or bending test.

Further studies will be investigated in the first instance to the identification in the geometrically non-linear approach from the critical point using stable branches solutions in terms of in-plane strains and in-plane curvatures. A continuation method as the Asymptotic Numerical Method (ANM) (Boutyour et al., 2004; Abdelkhalek et al., 2015) can be used to accurately determine the bifurcation point. Further work will be devoted to an experimental study by exposing

polymer matrix material sample to a humid environment and then carrying out deflection measurements for the identification of diffuso-mechanical properties in the transient regime. The conclusions of the present study will be used for designing a proper test (sample dimensions and humidity conditions) starting from the knowledge of the moisture dependent material properties identified by using traction tests.

Acknowledgments

This work pertains to the French Government program Investissements dAvenir (LABEX INTERACTIFS, reference ANR-11-LABX-0017-01). We acknowledge the support of the French Ministry of Education and Research for funding the PhD thesis of Anani Djato.

References

Abdelkhalek, S., Zahrouni, H., Legrand, N., Potier-Ferry, M., 2015. Post-buckling modeling for strips under tension and residual stresses using asymptotic numerical method. IJMS 104, 126–137.

Beringhier, M., Djato, A., Maida, D., Gigliotti, M., 2018. A novel protocol for rapid identification of anisotropic diffusion properties of polymer matrix composite materials with complex texture. Compos. Struct. 201, 1088 – 1096.

Boutyour, E. H., H, Z., Potier-Ferry, M., Boudi, M., 2004. Asymptotic-numerical method for buckling analysis of shell structures with large rotations. J. Comput. Appl. Math. 168, 77–85.

Djato, A., Beringhier, M., Gigliotti, M., 2018. Identification of moisture affected mechanical properties of polymer matrix materials by the employment of samples with moisture gradients. Mech. Adv. Mater. Struc. DOI: 10.1080/15376494.2018.1536933.

Fick, A., 1855. On liquid diffusion / ueber diffusion. Poggendorff's Annalen der Physik und Chemie 94, 58–86.

Gigliotti, M., Jacquemin, F., Molimard, J., Vautrin, A., 2007. Transient and cyclical hygrothermoelastic stress in laminated composite plates: Modelling and experimental assessment. Mech. Mater. 39, 729745.

Gigliotti, M., Minervino, M., 2014. The deformed shape of isotropic and orthotropic plates subjected to bending moments distributed along the edges. IJTAM 49, 1367–1384.

Gigliotti, M., Molimard, J., Jacquemin, F., Vautrin, A., 2006. On the nonlinear deformations of thin unsymmetric 0/90 composite plates under hygrothermal loads. Composites Part A 37, 624629.

Hyer, M. W., 1981. Calculation of the room-temperature shape of unsymmetric laminates. J. Compos. Mater. 15, 296–310.

Mansfield, E. H., 1989. The Bending & Stretching of Plates. Cambridge University Press.

Obeid, H., Clement, A., Freour, S., Jacquemin, F., Casari, P., 2018. On the identification of the coefficient of moisture expansion of polyamide-6: Accounting differential swelling strains and plasticization. Mech. Mater. 118, 1–10.

Ounaies, M., Harchay, M., Dammak, F., Daly, H. B., 2018. Prediction of hygrothermal behavior of polyester/glass fiber composite in dissymmetric absorption. J. Compos. Mater. 52, 4001–4007.

Shen, C.-H., Springer, G. S., 1976. Moisture absorption and desorption of composite materials. J. Compos. Mater. 10, 2–20.

Shen, C. H., Springer, G. S., 1977a. Effects of moisture and temperature on the tensile strength of composite materials. J. Compos. Mater. 11, 2–16.

Shen, C. H., Springer, G. S., 1977b. Environmental effects on the elastic moduli of composite materials. J. Compos. Mater. 11, 250–264.

Simar, A., 2014. Impact du vieillissement humide sur le comportement d'un composite à matrice organique tissé fabriqué par injection rtm : mise en évidence

d'un couplage entre absorption d'eau et thermo-oxydation de la matrice. Ph.D. thesis, Ecole Nationale Supérieure de Mécanique et d'Aéronautique (ENSMA).

Simar, A., Gigliotti, M., Grandidier, J.-C., Ammar-Khodja, I., 2014. Evidence of thermo-oxidation phenomena occurring during hygrothermal aging of thermosetting resins for rtm composite applications. Composites Part A: Appl. Sci. Manuf. 66, 175–182.

Weitsman, Y. J., 2012. Fluids Effects in Polymers and Polymeric Composites. Springer.

Youssef, G., Frour, S., Jacquemin, F., 2009. Stress-dependent moisture diffusion in composite materials. J. Compos. Mater. 43, 1621–1637.

Zara, F., 2017. Modèle mécanique d'une plaque mince. Ph.D. thesis, Université de Lyon.